Role of implantation temperature on residual damage in ion-implanted 6H-SiC

# Role of implantation temperature on residual damage in ion-implanted 6H–SiC

## R Héliou, J L Brebner[1] and S Roorda

Groupe de recherche en science et technologie des couches minces and
Département de physique, Université de Montréal, Montréal, Québec, Canada H3C-3J7

E-mail: sjoerd.roorda@umontreal.ca

## Abstract
The optical and structural properties of ion-implanted 6H–SiC single
crystals were investigated for samples implanted with 370 keV $^{28}$Si ions to
doses ranging from $5 \times 10^{13}$ to $1 \times 10^{16}$ cm$^{-2}$ and at irradiation
temperatures ranging from 20 to 600 °C. Rutherford backscattering
spectrometry channelling (RBS/C) showed that the dynamic recovery of the
induced-damage layer increases with irradiation temperature. The final
disorder determined from RBS/C as a function of implantation temperature
was modelled in terms of a thermally activated process which yielded an
activation energy of 0.08 eV. Defect distributions are found to shift to
greater depths with increasing implantation temperature and dose. Some
defects are even found farther than the accessible range of the implanted
ions. RBS/C data on high-temperature implantations also suggests that
defect complexes are created at high doses in addition to the point defects
that are still stable at high temperature. A decrease in Raman intensity of
implanted samples relative to that of crystalline samples was observed and
correlated with an increase in optical absorption near the wavelength of the
laser pump (514.5 nm).

## 1. Introduction

Because of its physical and electronic properties, such as
wide band gap, high breakdown electric field, high thermal
conductivity and high saturated electron drift velocity, silicon
carbide (SiC) has been widely studied in the last few
years. It is a promising semiconductor material for high-
temperature, radiation-resistant and high-power/frequency
electronic devices [1, 2].

Dopant incorporation is a major step in electronic device
fabrication. Due to low atomic mobilities in SiC, doping by
thermal diffusion is not practical [3]. Clearly, ion implantation
is an interesting alternative method provided the irradiation
damage can be annealed out. A fundamental understanding of
the dependence of residual implantation damage on irradiation
temperature is necessary to be able to effectively use ion
implantation.

The aim of this paper is to investigate changes in the
optical and structural properties of SiC as a function of

implantation dose and temperature. Rutherford backscattering
spectrometry channelling (RBS/C), Raman spectroscopy and
optical absorption were used to do so. Si was chosen as the
implantation ion so that there would be minimal changes in the
chemical structure of the SiC.

An activation energy calculation derived from the damage
recovery data with temperature is presented. Evidence
supporting the creation of more complex defects, at high doses
and temperatures, is discussed. A comparison in terms of
efficiency between dynamic annealing and post-implantation
thermal annealing is also made.

## 2. Experiment

Single-crystal 6H–SiC wafers (from Cree Research), 250 $\mu$m
thick, with (0001) orientation were used. Damaged surface
layers were produced by 370 keV Si$^+$ implantation with
different doses ($5 \times 10^{13}$ to $1 \times 10^{16}$ Si$^+$ cm$^{-2}$) and over a
temperature range of 20–600 °C. The implantations were made
at 7° off the [0001] axis with a mean current of 1.5 $\mu$A raster
scanned over an area of $1 \times 1$ cm$^2$. The energy of the implanted

---

[1] Deceased.
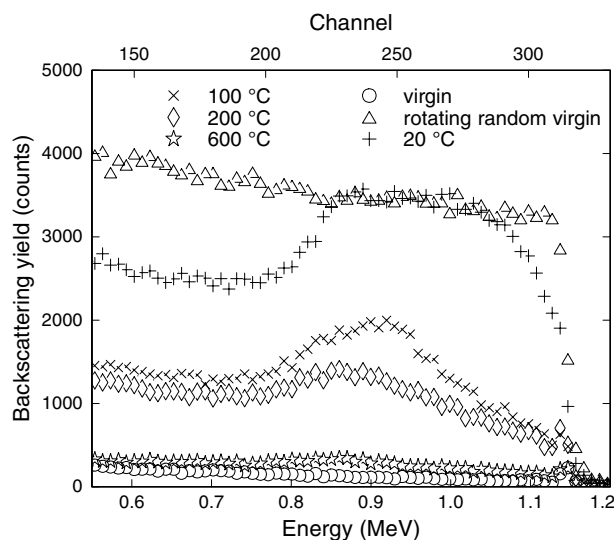
**Figure 1.** Typical RBS/C spectra channelled in the [0001] direction from a virgin sample and samples implanted with $1 \times 10^{15}$ Si$^+$ cm$^{-2}$ at different temperatures. A rotating random spectrum of a virgin sample is also included.

Si was chosen so that the projected ion range ($R_p$) would be 370 nm [4], making the damaged layers easily accessible for RBS. The wafers were cut into $1 \times 1$ cm$^2$ pieces, each piece containing an irradiated and an unirradiated area. A total of 28 pieces of SiC were implanted at seven temperatures with four different doses for each temperature. These doses were chosen to be near the critical dose for amorphization at a given temperature without changing the stoichiometry by more than 1%.

RBS/C analysis was performed with 2 MeV He$^+$ ions along the [0001] channelling direction at a backscattering angle of 170°. The beam current was kept between 6 and 8 nA.

Raman spectra were recorded with a U1000 ISA double spectrometer coupled with a CCD camera cooled at liquid nitrogen temperature. The 514.5 nm line of an argon ion laser was used in a backscattering geometry to observe Raman scattering. The laser intensity on the sample was about 40 mW, focused on a $1 \times 1$ mm$^2$ region. Illumination was incident at close to the perpendicular of the (0001) plane, but no effort was made to orient the sample with respect to the laser polarization. The optical absorption measurements were carried out with a Perkin Elmer Lambda 19 double spectrometer equipped with a halogen lamp (visible region) and a deuterium lamp (UV range) as light sources and a photomultiplier as the detector.

## 3. Results and discussion

### 3.1. RBS/C analysis

A set of typical RBS/C spectra obtained from samples implanted with $1 \times 10^{15}$ Si$^+$ cm$^{-2}$ at different temperatures is presented in figure 1; a spectrum of a randomly oriented virgin sample rotating around the [0001] axis and a channelled spectrum along the same sample axis are also shown. Because the channelled backscattering yield reduction was more evident in the Si signal, all calculations of displaced atoms were performed on that part of the spectrum.

The ratio of channelled to random crystalline spectra near the surface was about 3%, thus showing the good quality of the material. For each implanted sample this ratio increased with dose, but less so at higher implantation temperatures. The emergence of a damage peak in the channelling spectra indicates the presence of point defects which can cause direct backscattering of channelled ions and dechannelling. The distribution profile of these defects is not uniform, the maximum concentration varying in depth as a function of dose and temperature. The backscattering yield of the damaged layer reaches the random level only for the sample implanted with $1 \times 10^{15}$ Si$^+$ cm$^{-2}$ at room temperature (RT), hence this layer can be characterized as amorphous from a RBS/C viewpoint. This dose corresponds to 0.57 displacement per atom (dpa) at the maximum of the damage peak, as calculated from a Trim-97 simulation. Using transmission electron microscopy (TEM) measurements, Zinkle and Snead [5] found the amorphization threshold for 560 keV Si$^+$ at RT to be 0.55 dpa [5]. We therefore assume that the $1 \times 10^{15}$ Si$^+$ cm$^{-2}$ sample implanted at RT is truly amorphous and all other implanted samples are only partially damaged to different levels.

The thickness of the buried amorphous layer can be determined using the density of 6H–SiC (3.2 g cm$^{-3}$) and the energy width of the plateau region associated with the layer. The thickness is estimated to be about 440 nm. In the same way, we can calculate *the depth at maximum value of the damage peak* ($D_m$). This depth increases with temperature to well beyond $R_p$. Furthermore, in samples implanted at 600 °C at doses of $5 \times 10^{15}$ or $1 \times 10^{16}$ Si cm$^{-2}$, defects are present at depths greater than the range accessible to 370 keV Si ions. These $D_m$ increases could be caused by the formation of a thick SiO$_2$ layer at the surface which could modify the $D_m$ values by changing the reference point of the surface. However there is no evidence of oxygen in the RBS spectra of any implanted sample. Consequently, we can assume that these $D_m$ shifts with increasing dose and temperature are real. These effects may be due to an increase in the average diffusion length of the defects with implantation temperature and also to the presence of the sample's surface which acts as a trap and limits the defect diffusion, thus displacing the maximum of the defect distribution to greater depths. At each implantation temperature (except RT), the $D_m$ also increases with dose up to $5 \times 10^{15}$ Si$^+$ cm$^{-2}$. This is what we expect because a higher dose requires more time to implant. As for the temperature, an increase in the time allowed for the diffusion to take place also indicates an increase in the average diffusion length of the defects. An example of this kind of behaviour is shown in figure 2 for RBS/C spectra obtained from samples implanted at 500 °C with different doses. In this figure we plot the yield ratios for samples aligned and in a random position ($Y_{aligned}/Y_{random}$). However at RT, the $D_m$ is constant regardless of the dose. This last result has also been reported by other authors, but for different ion species [6,7].

For all samples implanted with $1 \times 10^{16}$ Si$^+$ cm$^{-2}$ at temperatures of 200 °C and higher, the shape of the channelled spectra appears to indicate the presence of two types of defect, with overlapping distributions. The new distribution appears to be immobile and centred at $R_p$. We suggest that in addition to point defects still stable at these temperatures, there are
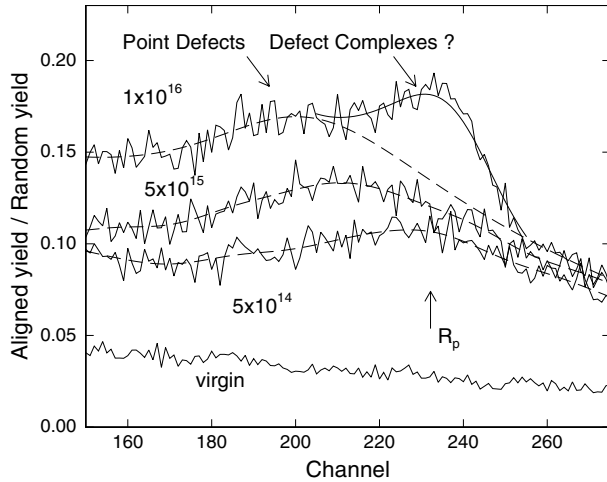
**Figure 2.** RBS/C spectra channelled in the [0001] direction from a virgin sample and samples implanted at 500 °C with different doses where we plot the yield ratios for samples aligned and in a random positions ($Y_{aligned}/Y_{random}$). The broken and full curves represent, respectively, guides to the eye for the point defect distribution shifts and the new distribution. The value of $R_p$ is also indicated on the figure.



**Figure 3.** Saturated disorder (in displaced Si atoms cm$^{-2}$), as calculated from RBS/C spectra, as a function of implantation temperature. An Ahrrenius-type fit with an activation energy of 0.08 eV is included. Inset: number of displaced Si atoms as calculated from RBS/C spectra as a function of dose for different implantation temperatures; the origin represents an unimplanted sample.

defect complexes being created at high doses (and possibly high temperatures) significantly less mobile than the initial point defects. Figure 2 also shows the evolution of the point defect distribution for doses up to $5 \times 10^{15}$ Si$^+$ cm$^{-2}$ and the emergence of the new distribution for the sample implanted with $1 \times 10^{16}$ Si$^+$ cm$^{-2}$. The broken and full curves represent, respectively, guides to the eye for the point defect distribution shifts and the new distribution.

$N_d \Delta x$, the number of displaced Si (in atoms cm$^{-2}$) in the crystal (representing the amount of disorder in the implanted layer) is determined from the *area under the damage Si peak*, $A_d$, relative to the *random level near the surface*, $H$, by the relation [8]

$$N_d \Delta x = (A_d \delta E)/(H[\varepsilon]) \tag{1}$$

where $N_d$ is the displaced atoms density, $\Delta x$ is the thickness of the damaged layer, $\delta E$ is the energy width of a channel in the backscattered spectrum and $[\varepsilon]$ is the stopping cross section. A straight-line approximation is used to account for dechannelling. The results for all implanted samples are reported as an inset in figure 3 where the disorder in the crystal (in atoms cm$^{-2}$) is plotted as a function of dose for different implantation temperatures. All curves pass through the origin which represents an unimplanted sample with no disorder.

This figure reveals that all samples implanted at temperatures higher than RT exhibit a region where the disorder reaches a plateau at high doses ($1 \times 10^{15}$ to $1 \times 10^{16}$ Si$^+$ cm$^{-2}$), the value at the plateau decreasing with increasing temperature. This plateau represents a saturation with ion dose of the quantity of defects still stable in the sample after implantation. The dynamic annealing during implantation favours defect recombination by giving enough energy to interstitial atoms to migrate to an equilibrium position in the crystal. The saturated disorder (an average taken over all doses forming the plateau representing the disorder saturation) is plotted against implantation temperature in figure 3. The uncertainties are calculated on the basis of
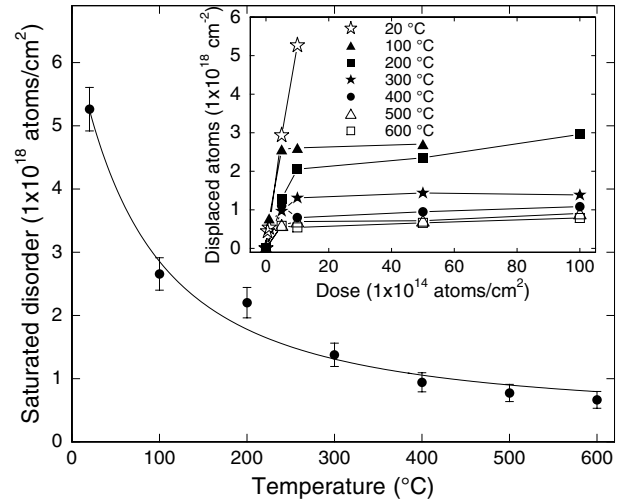
standard RBS statistics. An Arrhenius process fitted with an activation energy of $0.08 \pm 0.01$ eV is also included in figure 3. This energy is interpreted as a migration energy and is in good agreement with the activation energies measured by Weber *et al* [6]; the technique used by Weber *et al* was, however, different. By performing *in situ* TEM measurements they were able to measure, for various implantation temperatures, the dose needed for complete amorphization. A model developed to describe the temperature dependence of amorphization in ceramics and semiconductors in terms of a single activated process was then used to extract the activation energy [9, 10]. It is also to be noted that the energies discussed above are associated with a dynamic recovery process and not with post-implantation thermal recovery.

### 3.2. Raman analysis

A Raman spectrum of virgin SiC is shown in the inset of figure 4 where the Raman intensity is plotted against the wavenumber shift with respect to the laser. Because the highest intensity Raman lines are located between 700 and 1000 cm$^{-1}$, all measurements were carried out in that range. Four sharp lines are observed at 768, 789, 797 and 967 cm$^{-1}$. The 768 and 797 cm$^{-1}$ lines are, respectively, E$_2$ and E$_1$(TO) phonons. The 789 cm$^{-1}$ line is either an E$_2$ or an A$_1$(TO) phonon while the 967 cm$^{-1}$ is a combination of A$_1$(LO) and E$_1$(LO) vibrational modes [11]. The other curves in figure 4 will be discussed later.

Raman spectra were taken on the implanted and unimplanted parts of each sample. No shift or broadening of the lines was observed. There was no evidence of other lines or bands appearing after implantation, while no Raman signal could be detected for the amorphous sample. However, a decrease in Raman intensity with respect to the unirradiated part of the sample was observed and the lower the implantation temperature, the larger the reduction in the Raman intensity.
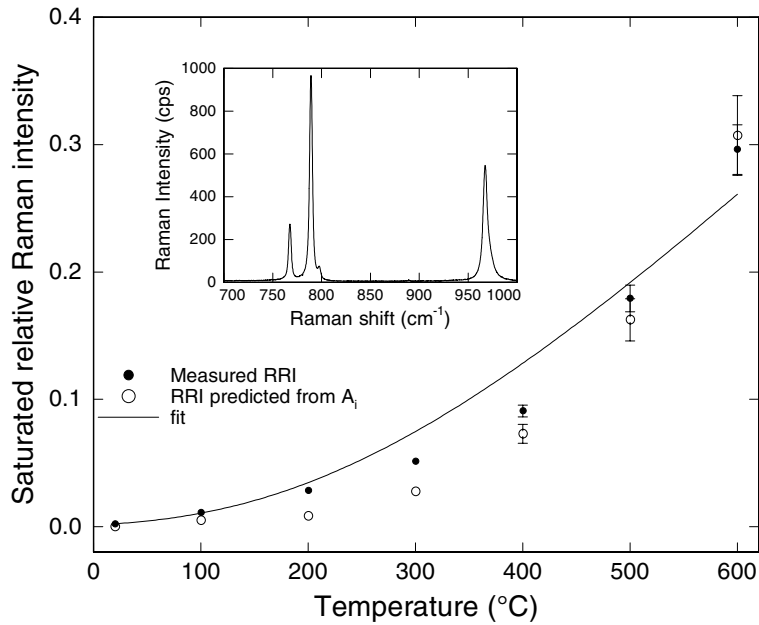
**Figure 4.** Comparison of measured and predicted saturated relative Raman intensity as a function of implantation temperature. An Ahrrenius-type fit with an activation energy of 0.27 eV is included. Inset: typical Raman spectrum of virgin 6H–SiC.

These observations suggest that the Raman signal mainly comes from the crystalline substrate underneath the implanted layers.

The relative Raman intensity ($RRI$) as a function of implantation dose for different implantation temperatures is also calculated and is shown in figure 5. Here $RRI$ means the Raman intensity of an implanted sample divided by the Raman intensity of the unimplanted part of the same sample averaged over the three most intense lines (768, 789 and 967 cm$^{-1}$). The point (0,1) is added to all curves and corresponds to an unimplanted sample. At low doses, the $RRI$ decreases monotonically only to saturate at higher doses. The saturated $RRI$'s (calculated by taking an average over all doses forming the plateau regions) are shown in figure 4 as functions of implantation temperature and are represented with full circles. The uncertainties were derived from the standard deviation for the intensity of a line in a typical Raman spectrum taken many times on the same sample. This deviation was found to be 5%. We see that the saturated $RRI$ increases exponentially with temperature and that it tends to zero at low temperatures and possibly to one at higher temperatures. The data seems to be of an Arrhenius type, but the fitting procedure gives a poorly defined activation energy and we can only conclude that the latter is less than 0.27 eV. This fit is included in figure 4 even if it does not represent the data very well. As shown below, the loss in Raman signal is due to increased optical absorption in the damaged layers. The last set of points (open circles) will be discussed in the following section.
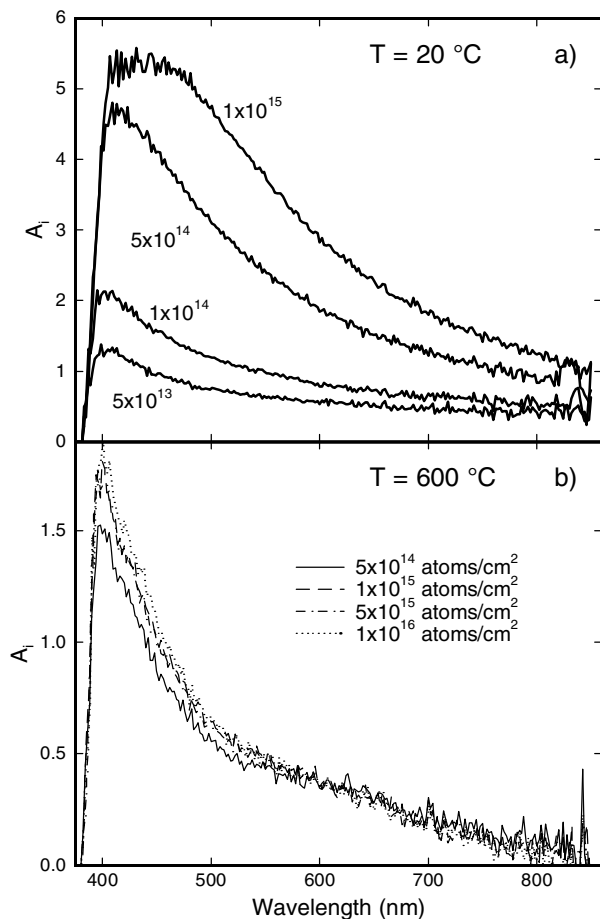
### 3.3. Optical absorption

The level of damage in the implanted samples was also followed by optical absorption in the UV and visible ranges. For each sample, the ratio $I/I_0$ was measured as a function of wavelength (between 200 and 860 nm), where $I$ is the
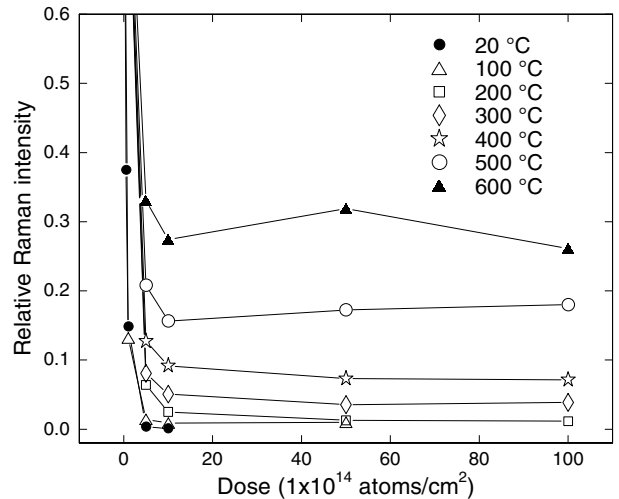


**Figure 5.** $RRI$ averaged over the three most intense lines as a function of dose for different implantation temperatures. An $RRI$ of one and a dose of zero correspond to an unimplanted sample.

intensity of the transmitted light and $I_0$ that of the incident beam. From the implanted and virgin measured $I/I_0$ ratios and Beer's law ($I/I_0 = (1 - R_c)(1 - R_a) \exp[-(A_i + A_c)]$ for an implanted sample where $A_c$ is the induced absorbance of an unimplanted sample), we can deduce the induced absorbance of the implanted layer ($A_i$) which is defined as the absorption coefficient of the damaged layer ($\alpha_i$) times the thickness of the layer. We make the approximation that the implanted samples consist of a thin implanted layer and the underlying substrate. Reflectances values of unimplanted ($R_c = 0.20$) and amorphous ($R_a = 0.28$) samples are based on the work of Musumeci *et al* [7] while all other implanted samples are accorded an intermediate reflectance $R_i = R_c + (A_i/A_a)(R_a - R_c)$, where $A_a$ is the absorbance of the amorphous sample.
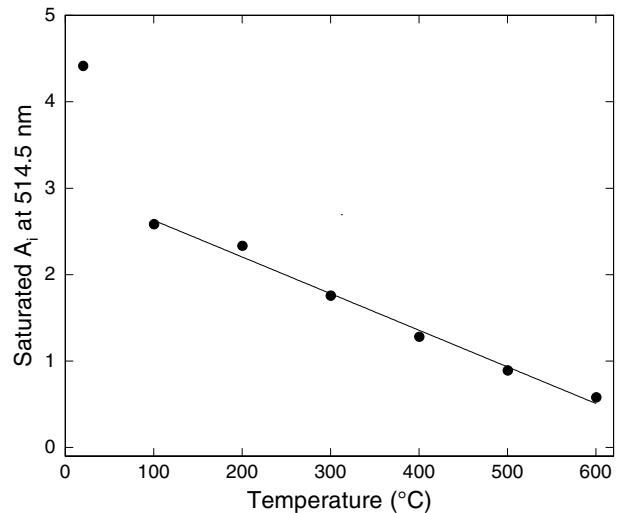
**Figure 7.** Saturated level of induced absorbance of the implanted layer as a function of implantation temperature. The full line is a least-squares fit of a straight line to all data points representing partially damaged layers.

**Figure 6.** Induced absorbance of the implanted layer ($A_i$) as a function of wavelength for samples implanted with different doses at RT (*a*) and at 600 °C (*b*).

$A_i$ measurements as a function of wavelength for samples implanted with different doses are reported in figure 6(*a*) for an implantation temperature of 20 °C and in figure 6(*b*) for 600 °C. In both figures a large absorption tail is detected following implantation, which is attributed to defect-related energy levels in the gap. The absorption increases with dose for constant temperature but again seems to be independent of dose at higher temperature. As the implantation temperature increases, the absorption tail becomes narrower, the tail curvature is more abrupt and the position of maximum absorption shifts towards higher energies.

To compare absorption and Raman measurements we calculated $A_i$ at the laser wavelength used for Raman spectroscopy (514.5 nm). For low doses, $A_i$ at 514.5 nm increases monotonically and then saturates at a certain dose ($>1 \times 10^{15}$ cm$^{-2}$) in the same way as RBS disorder or $RRI$. We can see more easily the effect of implantation temperature by calculating the saturated $A_i$ level at 514.5 nm. The results are shown in figure 7. The decrease in absorption is linear with temperature for damaged layers, while the RT implantation is a special case because of its amorphous state. For the same reasons as in the Raman case, an uncertainty of 5% was attributed for the ratios $I/I_0$. The uncertainties in figure 7 correspond roughly to the symbol size.

It is interesting to note how the amorphous sample ($1 \times 10^{15}$ Si$^+$ cm$^{-2}$ at RT) differs in terms of RBS and

absorption measurements. Figures 3 and 7 represent well the situation. In figure 3, we can see that in terms of the number of displaced Si atoms, the behaviour with implantation temperature is similar for amorphous and partially damaged layers. Even if we do not consider the point at 20 °C, the activation energy of the Arrhenius fit remains 0.08 eV. However, if we look at the two different types of layers produced by implantation (amorphous and damaged) in terms of absorption (figure 7), we see a clear difference. This may be caused by the fact that an amorphous sample has so many new energy levels available in the gap that intraband transitions start to contribute substantially to the absorption. This would greatly increase the level of absorption of an amorphous layer compared to a damaged one.

The data of figure 6 can also be used to correlate the decrease in intensity of the Raman signal in the implanted samples. If we assume (1) that the Raman signal originates from the crystalline part of the sample; (2) that because the implanted layer is much thinner than the substrate (0.37 $\mu$m over a total thickness of 250 $\mu$m), the Raman signal coming from a layer of that size, either before or after implantation, is negligible compared to the signal from the underlying substrate; and (3) that the loss in Raman signal is only caused by a reduction in intensity of the laser beam due to optical absorption in the implanted layer; then the $RRI$ should be related to $A_i$ according to

$$I_i/I_c = ((1 - R_i)/(1 - R_c))^2 \times \exp(-2A_i) \qquad (2)$$

where $I_i$ is the Raman intensity of an implanted sample and $I_c$ is the Raman intensity of a virgin sample. The factor of two originates from the reduction of the beam intensity by a factor $\exp(-A_i)$ when it traverses the implanted layer and another factor $\exp(-A_i)$ when it goes out of the sample to the detector. We can predict the ratio $I_i/I_c$ with equation (2) and $A_i$ measurements and compare this ratio to our Raman measurements. The results are shown in figure 4 and are represented by open circles. We see that the predicted $I_i/I_c$

ratios fit well with the Raman data, although it slightly underestimates the actual $RRI$'s. This is probably due to a partial contribution of the implanted layer to the Raman signal and an overestimation of $A_i$ due to light diffusion by defects or surface roughness.

### 3.4. Post-implantation annealing

It is also interesting to compare dynamic annealing and post-implantation annealing in terms of residual damage. To do so, single-crystal 6H–SiC wafers were implanted with 370 keV Si$^+$ and 225 keV C$^+$ both at a dose of $1 \times 10^{15}$ cm$^{-2}$ to preserve the stoichiometry in the crystal. The wafer characteristics and implantation conditions (including implantation temperature varying over a range of RT to 600 °C) were also identical to those described in the experiment section. The energies of the implanted species were chosen so that their respective $R_p$ would overlap at about 370 nm [4]. Following implantation, the samples were annealed in a conventional furnace under a gas flow of argon at 1000 or 1500 °C for 1 h. Thus, for each implantation temperature (RT, 200, 400 and 600 °C), we have three samples (1000 °C annealed, 1500 °C annealed or no annealing at all). RBS/C was performed on each implanted sample.

These implantations are very similar to those discussed in sections 3.1, 3.2 and 3.3. According to Trim-97, a Si implantation produces about three times more vacancies than a C implantation at these energies. Therefore, in terms of damage production (vacancies), a sequential implantation of $1 \times 10^{15}$ cm$^{-2}$ Si and C is equivalent to a single implantation of about $1.3 \times 10^{15}$ cm$^{-2}$ Si.

However, in these coimplantations, Si was always implanted before C. Therefore, one could ask whether the damage profile would be similar if C was implanted first. Some measurements were also carried out to try to answer this question and are discussed in the next section.

RBS/C measurements on the implanted and annealed samples reveal the additive effect of post annealing on residual damage after implantation at high temperature. RBS/C spectra taken on samples annealed at 1000 and 1500 °C, but previously implanted at RT and 600 °C are shown in figure 8(a) and 8(b) respectively. In figure 8(a), we can see that the implantation produced an amorphous region in the as-implanted sample. As discussed in section 3.1A, this layer can be considered as truly amorphous. Annealing at 1000 °C causes a decrease in the thickness of this amorphous layer. This decrease is even more pronounced than it appears because there is clearly some oxygen at the surface which further increases the energy loss of the impinging He ions. The oxygen surface peak at channel 190 and missing Si counts at the surface compared to the as-implanted sample proves that there is formation of a SiO$_2$ layer at the surface of the annealed sample. Although the annealing was performed under a gas flow of argon, there could have been some oxygen left in the furnace to start this oxidation process.

To prevent oxidation during the annealing procedure, the samples were placed face down on another piece of SiC, however since SiO$_2$ melts at 1200 °C, they were fused together during the 1500 °C annealing. A solution of 40% hydrofluoric acid (HF) was then used to separate them.
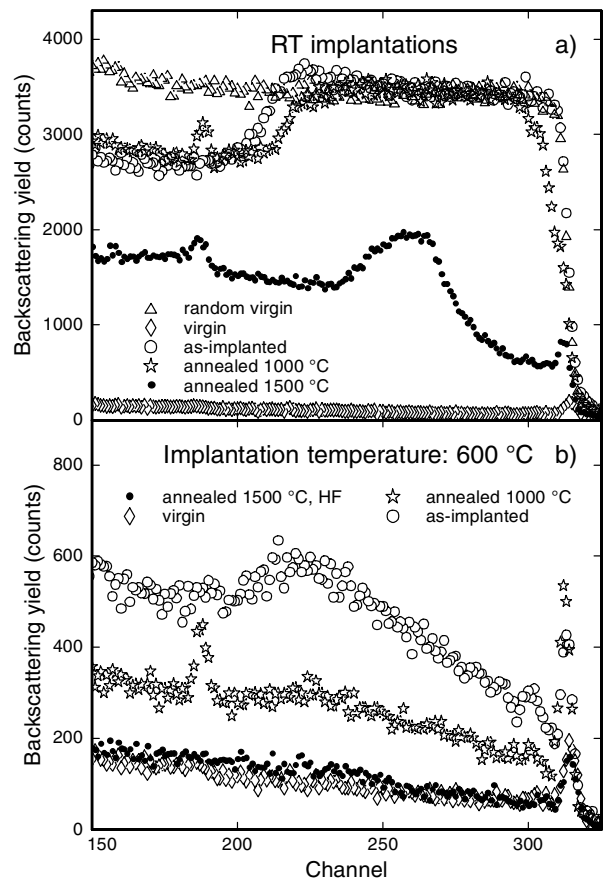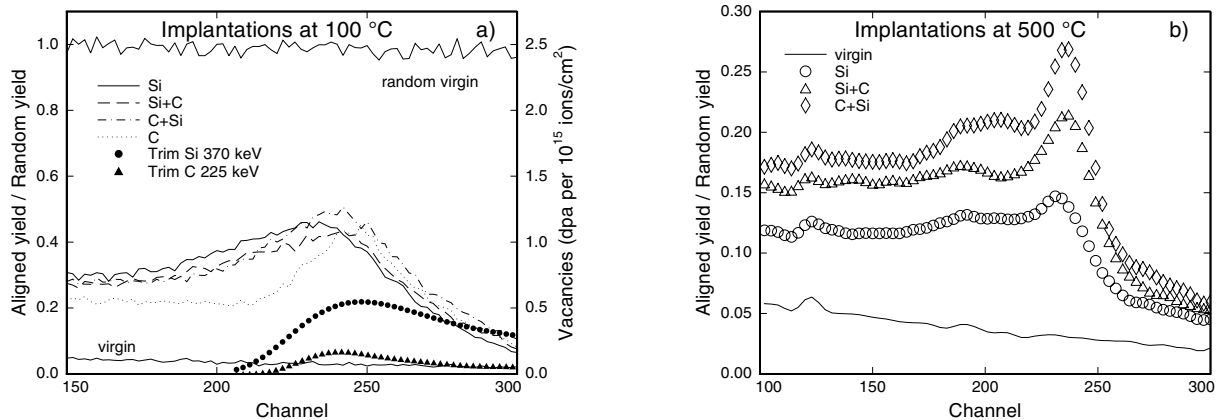


**Figure 8.** RBS/C spectra channelled in the [0001] direction from a virgin sample and samples implanted with $1 \times 10^{15}$ Si$^+$ cm$^{-2}$ and $1 \times 10^{15}$ C$^+$ cm$^{-2}$ at RT (a) and at 600 °C (b). Samples also annealed at 1000 °C, or annealed at 1500 °C and then etched in HF to remove the surface oxide, are also shown in both figures. A rotating random spectrum of a virgin sample is also included in (a).

This explains, for example, the thinner oxide layer on the 1500 °C annealed samples compared to those annealed at 1000 °C (see figure 8(a)). For this reason, the amount of oxygen seen in the RBS/C spectra in both figures does not represent what was really created during implantation. In any case, apart from the dechannelling caused by a surface SiO$_2$ layer, the oxidation should not affect the annealing behaviour. In fact, some measurements were carried out to verify this, as discussed below.

The effect of oxidation on the annealing behaviour in SiC was also studied by Bohn *et al* [12], who implanted Cr and N in 6H–SiC to create damage and then annealed their samples in a furnace at various temperatures. They did not, however, combine implantation at high temperature and post annealing. Bohn *et al* also found the presence of a surface SiO$_2$ layer after annealing. They carried out a special set of experiments to check if the oxidation had an influence on the annealing behaviour in SiC and found no change in the RBS/C spectra.

The RBS/C spectra in figure 8(a) for the sample annealed at 1500 °C clearly show that the damage is greatly reduced by the post annealing, as reported also by Bohn *et al* [12]. However, post-implantation anneals are not as effective as hot implants. There is four times more damage, in terms of backscattering, in the RT implantation followed by an

**Figure 9.** RBS/C spectra channelled in the [0001] direction from a virgin sample and samples implanted with Si only, C only, Si before C and C before Si all at an equivalent dose (in terms of displacement per atom) and at a temperature of 100 °C (*a*) and 600 °C (*b*). A rotating random spectrum of a virgin sample is included in (*a*). Vacancy profiles as calculated by a Trim-97 simulation for 370 keV Si and 225 keV C are also added in (*a*), these curves are associated with the scale on the right-hand side of the figure and are in units of displacement per atom for a dose of $1 \times 10^{15}$ cm$^{-2}$.

annealing at 1500 °C than in a simple implantation at 600 °C. As described in sections 3.1–3.3, implanting at temperatures higher than RT drastically reduces the residual damage, but does not remove it completely (in the temperature range investigated). We see again this kind of behaviour in figure 8(*b*) for the as-implanted (at 600 °C) and the implanted at 600 °C and annealed at 1000 °C samples. Moreover, there is an almost complete recovery for the sample annealed at 1500 °C that had previously been implanted at 600 °C. The damage peak has almost disappeared. The surface oxide was removed by etching the sample in a 40% HF solution for 25 min. Although not shown in the figure, all samples implanted at temperatures higher than RT (that is, 200 and 400 °C) exhibit this behaviour. We see that the backscattering yield of the spectra corresponding to this sample matches the yield of a virgin sample near the surface. However there still remains a very small fraction of in-depth defects.

*3.5. Order of implantation*

In order to establish if the order of implantation in coimplantations has an effect on the damage profile created in SiC, other 6H–SiC wafers were implanted with Si and C ions (with the same energies as discussed above). These implantations were made at two different temperatures, that is to say 100 and 500 °C. For each temperature, four types of implantations are possible: only Si, only C, Si before C and C before Si. The ion doses were chosen to create a defect distribution easily accessible with RBS/C and also such that the damage produced in the crystal, in terms of displacement per atom at the maximum of the damage peak, was identical in each four implantation scenarios. In the case of the 100 °C implantations, a total dose of 0.37 dpa was deposited. This is equivalent to $5 \times 10^{14}$ Si cm$^{-2}$ and $5 \times 10^{14}$ C cm$^{-2}$ (for coimplantations), $6.7 \times 10^{14}$ cm$^{-2}$ for Si only and $2 \times 10^{15}$ cm$^{-2}$ for C only. For implantations at 500 °C, doses of $1 \times 10^{16}$ Si cm$^{-2}$ and $1 \times 10^{16}$ C cm$^{-2}$ (for coimplantations) and $1.3 \times 10^{16}$ cm$^{-2}$ for Si only all correspond to a total dose of 7.4 dpa.

An analysis by RBS/C (always in the [0001] direction) was again performed on each implanted sample. We see in

figure 9(*a*) the results obtained with samples implanted at 100 °C and in figure 9(*b*) those implanted at 500 °C where, as in figure 2, we plot the yield ratios for an aligned sample and one in a random position. Figure 9 shows that no matter the sample's temperature, it is the implantation of C before Si that causes the most damage. The different defect distributions in figure 9(*a*) all have similar shapes, except the implantation of C only. The latter distribution is much narrower than the others and corresponds well with the vacancy profile predicted by Trim-97. Trim-97 vacancy profiles for 370 keV Si and 225 keV C are both included in figure 9(*a*). These profiles are in units of displacement per atom for a dose of $1 \times 10^{15}$ cm$^{-2}$. Their respective scale is on the right-hand side of the figure. Moreover, in the same figure we observe that every Si implantation created damage deeper than expected. The effect of dynamic annealing on the in-depth defects positions is then clearly visible. The diffusion of the Si defects created by the C-only implantation seems, however, less efficient.

We can also recognize in figure 9(*b*) the presence of a double distribution in each curve. In fact, this is the same phenomenon that was observed previously in section 3.1, which is, first, a distribution representing point defects diffusing toward greater depths and, second, another immobile distribution and centred at $R_p$, which possibly represents defect complexes. The necessary conditions for such a bimodal defect distribution are again: a high implantation temperature (500 °C) and a high dose ($1 \times 10^{16}$ Si cm$^{-2}$ and $1 \times 10^{16}$ C cm$^{-2}$).

We can therefore conclude that there is a systematic difference between the different orders of Si and C sequential implantations. For each implantation temperature, the C-before-Si implantation creates more damage than the Si-before-C implantation. This may be due to the higher defect production rate for the Si implantation (because of the lower ionic current for the C implantation) and, more importantly, because the effect of dynamic annealing would be reduced if the Si implantation was performed on a previously damaged SiC crystal. Thus, one has to be careful with the order of implantation, in terms of defect production, when implanting successively different ion species in SiC.

## 4. Conclusions

Residual damage in 6H–SiC single crystals after Si implantation at different temperatures has been followed by RBS/C, Raman spectroscopy and optical absorption.

The observed amount of disorder indicates damage recovery during implantation with an activation energy of $0.08 \pm 0.01$ eV. RBS/C data on high-temperature implantations also suggest that for doses of $1 \times 10^{16}$ Si$^+$ cm$^{-2}$, defect complexes are created in addition to point defects that are still stable at high temperature. The diffusion processes of these two types of defect are, however, different.

Optical absorption measurements have been used to correlate the decrease in $RRI$ as a function of temperature with an increase in absorbance of the damaged layer.

The combined effects of high-temperature implantation and post-implantation thermal annealing on residual damage were also studied by RBS/C. The data show that residual damage is almost completely removed after implantation at a temperature of 200 °C or higher and an annealing at 1500 °C for 1 h in an argon atmosphere.

## Acknowledgments

## References

[1] Celnokov V E 1992 *Mater. Sci. Eng.* B **11** 103
[2] Shnai K, Scott R S and Baliga B J 1989 *IEEE Trans. Electron Devices* **36** 1811
[3] Davis R F, Kelner G, Shur M, Palmour J W and Edmond J A 1991 *Proc. IEEE* **79** 677
[4] Ziegler J F and Biersack J P 1985 *The Stopping and Range of Ions in Solids* (New York: Pergamon)
[5] Zinkle S J and Snead L L 1996 *Nucl. Instrum. Methods* B **116** 92
[6] Weber W J, Wang L M, Yu N and Ness N J 1998 *Mater. Sci. Eng.* A **253** 62
[7] Musumeci P, Calcagno L, Grimaldi M G and Foti G 1996 *Nucl. Instrum. Methods* B **116** 327
[8] Swanson M L 1995 *Handbook of Modern Ion Beam Materials Analysis* ed J R Tesmer and M Nastasi (Pittsburgh, PA: Materials Research Society) p 271
[9] Weber W J, Ewing R C and Wang L M 1994 *J. Mater. Res.* **9** 688
[10] Weber W J and Wang L M 1994 *Nucl. Instrum. Methods* B **91** 63
[11] Feldman D W, Parker J H, Choyke W J and Patrick L 1968 *Phys. Rev.* **170** 698
[12] Bohn H G, Williams J M, McHargue C J and Begun G M 1987 *J. Mater. Res.* **2** 107